This article has been accepted for publication in a future issue of this journal, but has not been fully edited. Content may change prior to final publication. Citation information: DOI 10.1109/TCOMM.2017.2751552, IEEE Transactions on Communications

DNA-GA: A Tractable Approach for Performance Analysis of Uplink Cellular Networks

Ming Ding, *Senior Member, IEEE*, David López Pérez, *Senior Member, IEEE*, Guoqiang Mao, *Senior Member, IEEE*, Zihuai Lin, *Senior Member, IEEE*, and Sajal K. Das, *Fellow, IEEE*

***Abstract*—In this paper, we propose a tractable semi-analytical approach for network performance analysis of uplink (UL) cellular networks, which is based on a deterministic network analysis using a Gaussian approximation (DNA-GA). The key contribution of this work is to investigate the UL signal-to-interference ratio (SIR) performance using the DNA-GA analysis. In particular, the SIR is modeled as a *ratio* of two random variables (RVs), representing the signal power and the aggregate interference power, respectively. The signal power is further characterized by a *product* of two RVs, i.e., a lognormal RV and a RV with an arbitrary distribution. The former RV comes from a common assumption of lognormal shadow fading, and the latter one takes the rest of random factors into account, such as random user positions, arbitrary types of multi-path fading, etc. The aggregate interference power is approximated by a RV with a power lognormal distribution. The proposed DNA-GA analysis has a few desirable features: (i) it naturally considers lognormal shadow fading; (ii) it can treat arbitrary shape and/or size of cell coverage areas; (iii) it can handle non-uniform user distributions; (iv) it can cope with any type of multi-path fading; (v) it can be applied to multi-antenna base stations (BSs). These features make the DNA-GA analysis very useful for network performance analysis of the 5th generation (5G) systems with general cell deployment and user distribution.**

***Index Terms*—uplink, signal-to-interference ratio (SIR) analysis, small cell networks (SCNs), Gaussian, approximation, lognormal, power lognormal.**

I. Introduction

From 1950 to 2000, the wireless network capacity has increased around 1 million fold, in which an astounding 2700× gain was achieved through network densification using smaller cells [1]. In the first decade of 2000, network densification continued to fuel the 3rd Generation Partnership Project (3GPP) 4th-generation (4G) Long Term Evolution (LTE) networks, and is expected to remain as one of the main forces to drive the 5th-generation (5G) networks onward [2]. In general, four network scenarios (NSs) with difference base station (BS) deployments can be found in the literature as shown in Fig. 1:

- **NS 1**: Full-coverage NS with BSs deployed on a hexagonal lattice, as illustrated in Fig. 1a.
- **NS 2**: Full-coverage NS with BSs deployed randomly, as illustrated in Fig. 1b.
- **NS 3**: Hotspot NS with BSs deployed on a hexagonal lattice, as illustrated in Fig. 1c, where hotspot areas are depicted by non-overlapping disk areas.
- **NS 4**: Hotspot NS with BSs deployed randomly, as illustrated in Fig. 1d, where hotspot areas are depicted by possibly overlapping disk areas.

In Fig. 1, BSs are represented by markers "x" and cell coverage areas for user equipment (UE) distribution are outlined by solid lines. Note that NS 1 has been widely used to model macrocell networks and the rest of the NSs have been considered for small cell networks (SCNs) [2], [3]. For a practical 4G and 5G SCN, the 3GPP prefers NS 4 over NS 2 in the modeling of SCNs, since operators mainly use SCNs for capacity boosting or black spot removal in certain areas, not for overall coverage provision. It is important to note that the UE distribution is particularly difficult to characterize for NS 4. This is because, although the basic shape of each small cell coverage area is a disk in Fig. 1d, the coverage areas of most small cells are of irregular shape due to possible overlapping of disks caused by the random positions and the closeness of small cell BSs.

Regarding the relationship between macrocells and small cells, in practical 4G and 5G networks, there are two types of heterogeneous network (HetNet) deployments as follows:

- **Co-channel deployment**: macrocells and small cells operate on the *same* frequency spectrum (3GPP Small Cell Scenario #1 [3])
- **Orthogonal deployment**: macrocells and small cells operate on *different* frequency spectrum (3GPP Small Cell Scenario #2a [3])

For the co-channel deployment, a practical assumption is that macrocells and small cells are deployed according to NS 1 and NS 4, respectively. The combination of NS 1 and NS 2 might not be very practical because operators do not want to waste money providing double blanket coverage on the same frequency spectrum. For the orthogonal deployment, macrocells and small cells can be studied separately, and the 3GPP prefers NS 4 over NS 2 in the modeling of SCNs,

Manuscript received xxx xx, 2016; revised xxx xx, 2017; accepted xxx xx, 2017. Preliminary results related to this paper were presented at IEEE International Conference on Communications (ICC) 2017 [17]. The associate editor coordinating the review of this paper and approving it for publication was Prof. Jinhong Yuan.

Ming Ding is with Data61, CSIRO, Sydney, N.S.W. 2015, Australia (e-mail: Ming.Ding@data61.csiro.au).

David López-Pérez is with Nokia Bell Labs, Blanchardstown, Dublin 15, Ireland (email: dr.david.lopez@ieee.org).

Guoqiang Mao is with the School of Computing and Communication, University of Technology Sydney, Ultimo, N.S.W. 2007, Australia, and also with Data61, CSIRO, Sydney, N.S.W. 2015, Australia (e-mail: g.mao@ieee.org).

Zihuai Lin is with the School of Electrical and Information Engineering, The University of Sydney, Sydney, N.S.W. 2006, Australia (e-mail: zihuai.lin@sydney.edu.au).

Sajal K. Das is with the Department of Computer Science, Missouri University of Science and Technology, Rolla, MO 65409-0350, USA (e-mail: sajaldasuta@gmail.com).

Digital Object Identifier xx.xxxx/TOC.2017.xxxxxxx

This article has been accepted for publication in a future issue of this journal, but has not been fully edited. Content may change prior to final publication. Citation information: DOI 10.1109/TCOMM.2017.2751552, IEEE Transactions on Communications

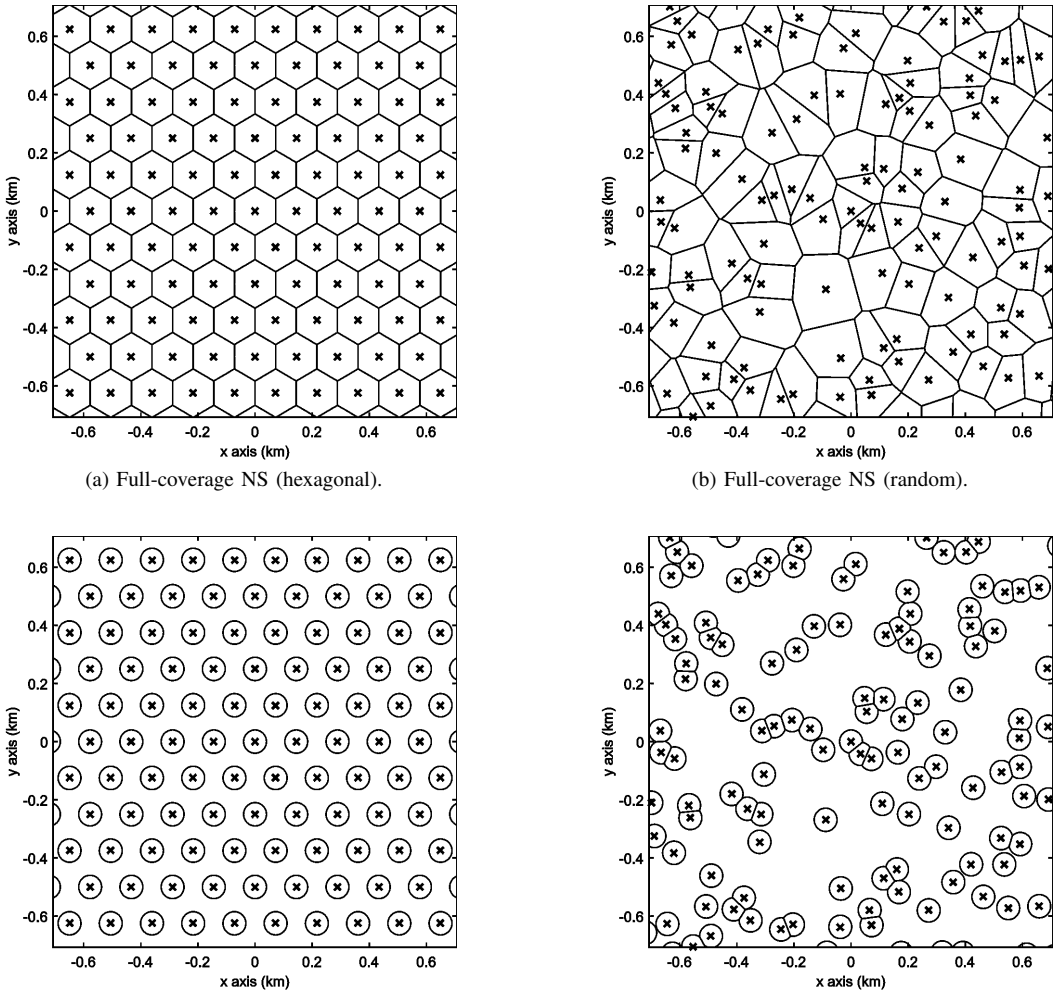

(a) Full-coverage NS (hexagonal).

(b) Full-coverage NS (random).

(c) Hotspot NS (hexagonal).

(d) Hotspot NS (random).

Fig. 1: Illustration of four network scenarios (NSs). Here, BSs are represented by markers "x" and cell coverage areas for user equipment (UE) distribution are outlined by solid lines.

as discussed before. Although the co-channel deployment provides a larger spatial reuse of spectrum than the orthogonal deployment, the future of dense SCNs lies with the orthogonal deployment[1], mainly because of the easy management, thanks to its low interaction with the macrocell tier, e.g., no inter-tier interference [2]. Hence, in this paper, we aim for the future and focus on the orthogonal deployment of SCNs within macrocells, which agrees with the view of many major operators around the world. As a result, the study of SCNs can be decoupled from that of macrocells, thus we do not consider the macrocell tier hereafter.

In this context, new and more powerful network performance analysis tools are needed to better understand the performance implications that these new dense orthogonal SCNs bring about [5]–[14]. Network performance analysis tools can be broadly classified into two categories, i.e., *macroscopic* analysis [5], [6] and *microscopic* analysis [7]–[14]. In a nutshell, the macroscopic analysis presents a general picture of the network performance, while the microscopic analysis gives more detailed results for specific networks. A more detailed explanation of these two analyses is provided in the following:

- The macroscopic analysis usually assumes that UEs and/or BSs are randomly deployed, often following a homogeneous Poisson distribution to invoke the use of the stochastic geometry theory [5], [6]. Such SCN is usually characterized by NS 2, as illustrated in Fig. 1b. In essence, the macroscopic analysis investigates network performance metrics at a high level, such as the coverage probability and area spectral efficiency, by averaging the performance results over all possible UE and BS deployments [5], [6]. The macroscopic analysis is particularly useful when an operator wants to know *the average performance across its whole network*.
- In contrast, the microscopic analysis allows for a more detailed analysis and is often conducted assuming that

[1]In more detail, the co-channel deployment requires cell range expansion (CRE) and time-domain enhanced inter-cell interference coordination (eICIC) to ensure successful macrocell off-loading and coping with the inter-tier interference issues [4]. The main drawback of the co-channel deployment with dense SCNs is that the macrocell tier will be practically muted due to the time-domain eICIC mechanism [2], which protects a very large number of small cells. The orthogonal deployment, on the other hand, calls for no eICIC operation and is easy to implement in practice.

This article has been accepted for publication in a future issue of this journal, but has not been fully edited. Content may change prior to final publication. Citation information: DOI 10.1109/TCOMM.2017.2751552, IEEE Transactions on Communications

UEs are randomly placed in the entire network or in hotspots, but that BS locations are known [7]–[14]. Such SCN is usually depicted by NS 3 or NS 4 in Fig. 1. In essence, the microscopic analysis is useful for a network-specific study and optimization, e.g., optimizing the interference cancellation parameters for a specific SCN [14]. In other words, the microscopic analysis can reveal the performance results for each individual network scenario before they are averaged to form a single performance result in the macroscopic analysis. The microscopic analysis is particularly useful when an operator wants to know *the performance of a specific BS deployment in its network or the performance impact of adding several specific BSs to its network*.

Within the microscopic analysis and paying special attention to the uplink (UL) SCNs, the authors in [7], [8] considered multiple UL interfering cells with disk-shaped coverage areas and presented closed-form expressions for the UL interference. In [9], [10], the authors conjectured that the UL interference in a hexagonal grid based cellular network should follow a lognormal distribution, which was verified via simulation. In [11], [12], the authors went a step further and derived an upper bound of the error in approximating the single-cell UL interference (in dB unit) by a Gaussian distribution [12], [15]. On the basis of this single-cell interference analysis, the distribution of the aggregate UL interference in a multi-cell scenario was approximated by a power lognormal distribution in [12]. For more practical and complex networks, in [13], [14], the authors investigated the network performance of SCNs in current 4G networks using system-level simulations.

Due to its generality and analytical tractability, the interference analysis based on the power lognormal distribution [12] promises a new way to analyze the UL signal to interference ratio (SIR), which has not been explored before and is the focus of this work. Since our work is based on a deterministic network analysis (DNA) using a Gaussian approximation (GA), the proposed analysis will be referred to as the DNA-GA analysis hereafter, and it comprises the following three steps:

1) The aggregate interference power is approximated by *a random variable (RV) with a power lognormal distribution* as in [11].
2) The signal power is characterized by a product of two RVs, i.e., *a lognormal RV* and *a RV with an arbitrary distribution*. The former RV comes from a common assumption of lognormal shadow fading. The distribution of such signal power RV is derived in tractable expressions using the Gauss-Hermite numerical integration [16].
3) The UL SIR is then modeled as a RV, which takes the form of $\frac{\text{a lognormal RV}\times\text{an arbitrary RV}}{\text{a power lognormal RV}}$ and its distribution is derived in this paper with tractable expressions.

Based on the above derivation, we present a single contribution in this paper[2]:

- *We make the DNA-GA analysis a tractable semi-analytical approach in the microscopic analysis family* with the following features:
  - it naturally considers lognormal shadow fading;
  - it can treat arbitrary shape and/or size of cell coverage areas;
  - it can handle non-uniform user distributions;
  - it can cope with any type of multi-path fading;
  - it can be applied to multi-antenna BSs.

Note that previously the DNA-GA analysis did not qualify as a functional microscopic analysis because it was able to analyze the aggregate interference only [12], not SIR. As explained earlier, it is non-trivial to derive the distribution of a SIR RV, which takes the form of $\frac{\text{a lognormal RV}\times\text{an arbitrary RV}}{\text{a power lognormal RV}}$ with each component having a complicated distribution function. Hence, our contribution in this work is distinctively different than that in our previous work [12], which focused on studying the approximation of the aggregate interference only.

The remainder of the paper is structured as follows. In Section II, we provide a brief review of the related work. In Section III, the network scenario and the wireless system model are described. In Section IV, the DNA-GA analysis is presented, followed by discussion on some special use cases of the DNA-GA analysis in Section IV-D. Our results are validated via simulations in Section V. Finally, the conclusions are drawn in Section VI.

II. Related Work

For the UL microscopic analysis, the existing work relies on the following approaches:

- **Approach 1: The analytical approach for small-scale networks**, which provides closed-form but complicated analytical results for a network with *multiple interfering cells, where each cell has a regularly-shaped coverage area*, e.g., a disk or a hexagon [7], [8]. Specifically in [8], the authors studied one UL interfering cell with a disk-shaped coverage area and presented closed-form expressions for the UL interference considering path loss, shadow fading, multi-path fading and BS scheduling.
- **Approach 2: The approximately analytical approach for lattice networks**, which first analyzes the UL interference and then makes an empirical assumption on the UL interference distribution, and on that basis derives analytical results for a network with *multiple interfering cells, whose BSs are placed on a regularly-shaped lattice*, e.g., a hexagonal lattice [9], [10]. Specifically in [10], the authors assumed that the uplink interference in an OFDMA-based hexagonal grid cellular network should follow a lognormal distribution. Such assumption was verified via simulation. In [9], the authors showed that the lognormal distribution better matches the distribution of the uplink interference in code division multiple access (CDMA) SCNs than the conventionally assumed Gaussian distribution in a hexagonal cellular layout.
- **Approach 3: The simulation approach for complex networks**, which conducts system-level simulations to directly obtain empirical results for a complex network

[2]Note that preliminary results of our work were presented in a conference paper [17].

This article has been accepted for publication in a future issue of this journal, but has not been fully edited. Content may change prior to final publication. Citation information: DOI 10.1109/TCOMM.2017.2751552, IEEE Transactions on Communications

with *practical deployment of multiple cells, whose BSs are placed at irregular locations* [2], [13], [14]. Specifically in [2], [13], [14], the authors conducted system-level simulations to investigate the network performance of SCNs in existing 4G networks and in future 5G networks.

In general, Approach 1 does not scale very well with dense SCNs and Approach 3 lacks analytical rigor. Regarding Approach 2, it has been a number of years since an empirical conjecture was extensively used in performance analysis, which stated that the UL inter-cell interference with *disk-shaped* coverage areas and *uniform UE distributions* could be well approximated by a lognormal distribution in CDMA SCNs [9] and in FDMA SCNs [10]. This conjecture is important since the lognormal approximation of interference distribution allows for tractable interference analysis with simple expressions, which forms an essential step of network performance analysis. In our previous works [11], [12], we verified such conjectures and answered the fundamental question of *how accurate* this lognormal approximation is, which paves the way to the SIR analysis, which will be the focus of this work.

III. Network Scenario and Wireless System Model

In this paper, we consider UL transmissions, and assume that each small cell BS only schedules *one* UE in each frequency/time resource, i.e., resource block (RB). This is a reasonable assumption in line with the 4G networks, i.e., Long Term Evolution (LTE) [3]. Note that small cells serving no UE are ignored in our analysis because no UL interference is generated from those small cells.

A. Network Scenario

Regarding the network scenario, we consider a SCN with multiple small cells operating on the same carrier frequency, as shown in Fig. 2. In more detail, the SCN consists of B small cells, each of which is managed by a BS. The network includes the small cell of interest denoted by C_1 and $B-1$ interfering small cells denoted by $C_b, b \in \{2,\ldots,B\}$. Note that as discussed in Section I, macrocells are not considered in our analysis since they are assumed to operate on different frequency spectrum from the SCN, i.e., orthogonal deployment.

We focus on a particular RB, and denote by K_b the active UE associated with small cell C_b transmitting on such RB. Moreover, we denote by R_b *the coverage area* of small cell C_b, in which its associated UEs are randomly distributed. Note that the coverage areas of adjacent small cells may share boundary due to the arbitrary shapes and sizes of $\{R_b\}, b \in \{2,\ldots,B\}$.

The distance (in km) from the BS of C_b to the BS of C_1, $b \in \{1,\ldots,B\}$, and the distance from UE K_b to the BS of C_m, $b,m \in \{1,\ldots,B\}$, are denoted by D_b and d_{bm}, respectively. Since the DNA-GA analysis belongs to the microscopic analysis family, we consider a deterministic deployment of BSs, i.e., the set $\{D_b\}$ is known, while UE K_b is randomly distributed in R_b with a probability density function (PDF) $f_{Z_b}(z)$, where $0 < f_{Z_b}(z) < +\infty, z \in R_b$ and its integral over R_b equals to one, i.e., $\int_{R_b} f_{Z_b}(z)\,dz = 1$. Hence, d_{bm} is a random variable (RV), whose distribution cannot be readily expressed in an analytical form due to the arbitrary shape and size of R_b, and the arbitrary form of $f_{Z_b}(z)$.

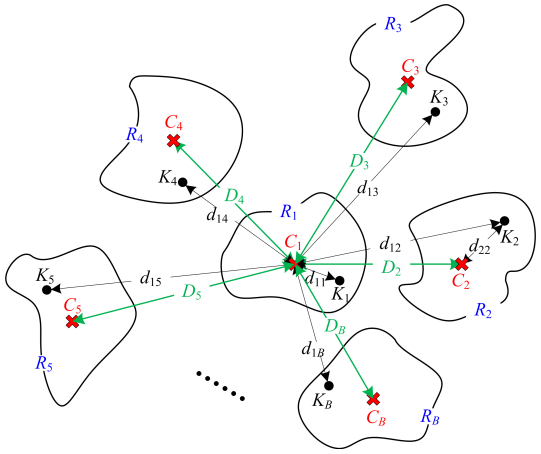

Fig. 2: A schematic diagram of the considered SCN.

B. Wireless System Model

Next, we present the modeling of path loss, shadow fading, UL transmission power, multi-path fading and multi-antenna reception filter, respectively.

Based on the definition of d_{bm}, *the path loss* in dB from UE K_b to the BS of C_m can be modeled as

$$L_{bm} = A + \alpha \times 10\log_{10} d_{bm}, \tag{1}$$

where A is the path loss in dB at the reference distance of $d_{bm} = 1$ and α is the path loss exponent. In practice, A and α are constants obtainable from field tests [18]. Note that L_{bm} is a RV due to the randomness of d_{bm}.

The shadow fading in dB from UE K_b to the BS of C_m is denoted by $S_{bm}, b,m \in \{1,\ldots,B\}$, where S_{bm} is usually assumed to follow a Gaussian distribution [18]. Based on this assumption, S_{bm} is modeled as an independently and identically distributed (i.i.d.) zero-mean Gaussian RV with a variance of σ^2_{Shad}, i.e., $S_{bm} \sim \mathcal{N}\left(0, \sigma^2_{\text{Shad}}\right)$. Note that a more realistic assumption would be the correlated shadow fading [19], which constructs S_{bm} and S_{jm} $(b,j,m \in \{1,\ldots,B\}, b \neq j)$ as correlated RVs, where the correlation coefficient decreases with the increase of the distance from UE K_b to UE K_j. Such assumption of the correlated shadow fading complicates the analysis since it is difficult to characterize the distribution of the inter-UE distance. For the sake of tractability, in this paper, we assume i.i.d. shadow fading for the UE-to-BS links.

The UL transmission power in dBm of UE K_b is denoted by P_b, and is subject to a semi-static power control (PC) mechanism, i.e., the fractional path loss compensation (FPC) scheme [18]. Based on this FPC scheme, P_b is modeled as

$$P_b = P_0 + \eta\left(L_{bb} + S_{bb}\right), \tag{2}$$

where P_0 is the target received power in dBm on the considered RB at the BS, $\eta \in (0,1]$ is the FPC factor, and

This article has been accepted for publication in a future issue of this journal, but has not been fully edited. Content may change prior to final publication. Citation information: DOI 10.1109/TCOMM.2017.2751552, IEEE Transactions on Communications

L_{bb} and $S_{bb} \sim \mathcal{N}\left(0, \sigma^2_{\text{Shad}}\right)$ have been discussed above. Note that in practice P_b is also constrained by the maximum value of the UL power, denoted by $P_{\max}$ at the UE. However, the power constraint is a minor issue for UEs in 5G dense SCNs since they are generally not power-limited due to the close proximity of a UE and its associated SCN BS. For example, it is recommended in [18] that $P_{\max}$ is smaller than the SCN BS downlink (DL) power by only 1 *dB*, which grants a similar outreach range of signal transmission for the BS and the UE. Therefore, the UL power limitation is a minor issue as long as the UE is able to connect with the serving BS in the DL. If the UE cannot establish a DL connection with the serving BS, then it is not very meaningful to consider the UL power constraint issue since the UL connection cannot exist without the assistance of the DL control signaling. For the sake of tractability, in this paper, we model P_b as (2), which has been widely adopted in the literature [5]–[8].

The multi-path fading channel vector from UE K_b to the BS of C_m is denoted by $\mathbf{h}_{bm} \in \mathbb{C}^{N^{\text{BS}} \times 1}, b, m \in \{1, \ldots, B\}$, where we assume that each UE is equipped with one omni-directional transmission antenna and each BS is equipped with N^{BS} reception antennas. As for the multi-antenna reception filter at the BS of C_m, we adopt the widely-used *normalized maximal ratio combining (MRC) reception filter* given by $\mathbf{f}_m = \frac{\mathbf{h}^{\text{H}}_{mm}}{\|\mathbf{h}_{mm}\|}$ [20], where $\mathbf{h}^{\text{H}}_{mm}$ is the Hermitian transpose of $\mathbf{h}_{mm}$ and $\|\mathbf{h}_{mm}\|$ is the Euclidean norm of $\mathbf{h}_{mm}$. It is important to note that we consider a general type of multi-path fading by assuming that the effective channel gain in dB associated with $\mathbf{h}_{bm}$ is defined as

$$H_{bm} = 10 \log_{10} W_{bm}, \ (b, m \in \{1, \ldots, B\}), \tag{3}$$

where W_{bm} is the effective channel gain of the link from UE K_b to the BS of C_m and it is expressed as [20]

$$W_{bm} = \left\|\mathbf{f}_m \mathbf{h}_{bm}\right\|^2. \tag{4}$$

The PDF and the CDF of H_{bm} are respectively denoted by $f_{H_{bm}}(h)$ and $F_{H_{bm}}(h)$, and they can be derived analytically according to the distribution of W_{bm}. For example, when $N^{\text{BS}} = 1$, W_{bm} can be characterized by an identically and independently distributed (i.i.d.) exponential distribution or a Gamma distribution in the case of Rayleigh fading or Nakagami fading, respectively [20]. As another example, when $N^{\text{BS}} \geq 1$ and with the consideration of Rayleigh fading, W_{mm} follows a chi-squared distribution with $2N^{\text{BS}}$ degrees of freedom [20] and $W_{bm}, (b \neq m)$ follows an i.i.d. exponential distribution with a mean of one [14].

Finally, we ignore the additive *noise* because the 4G/5G SCNs generally work in the interference-limited region [2]. Moreover, we assume that L_{bm}, S_{bm} and H_{bm} are independently distributed RVs as recommended by the 3GPP [18].

For clarity, the defined RVs in our system model are summarized in Table I.

IV. The Proposed DNA-GA Analysis

The proposed DNA-GA analysis consists of three steps, i.e., the interference power analysis, the signal power analysis, and the SIR analysis, which are presented in the following subsections. For clarity, we would like to summarized the key points of these analyses:

- *The interference power analysis* was presented in our previous work [12], where the aggregate interference power is approximated by *a RV with a power lognormal distribution*.
- *The signal power analysis* is completely different from [12]. More specifically, the signal power is characterized by a product of two RVs, i.e., *a lognormal RV* and *a RV with an arbitrary distribution*. The distribution of such signal power RV is derived in tractable expressions using the Gauss-Hermite numerical integration [16].
- *The SIR analysis* involves the treatment of the UL SIR, which is modeled as a complicated RV taking the form of $\frac{\text{a lognormal RV} \times \text{an arbitrary RV}}{\text{a power lognormal RV}}$. Its distribution is derived in this paper with tractable expressions.

A. The Interference Power Analysis

Based on the definition of RVs presented in Section III, *the UL received interference power* in dBm from UE K_b to the BS of C_1 can be written as

$$\begin{aligned} I_b &\overset{(a)}{=} P_b - L_{b1} - S_{b1} + H_{b1} \\ &= P_0 + \underbrace{(\eta L_{bb} - L_{b1})}_{L_b} + \underbrace{(\eta S_{bb} - S_{b1})}_{S_b} + H_{b1} \\ &= \underbrace{(P_0 + L_b + S_b)}_{I_b^{(1)}} + H_{b1} \\ &= I_b^{(1)} + H_{b1}, \end{aligned} \tag{5}$$

where (2) is plugged into the step (a) of (5), and L_b and S_b are defined as $L_b = (\eta L_{bb} - L_{b1})$ and $S_b = (\eta S_{bb} - S_{b1})$, respectively. As discussed in Subsection III-B, L_b and S_b are *independent* RVs. Besides, the first part of I_b is further defined as $I_b^{(1)} = (P_0 + L_b + S_b)$. Since S_{bb} and S_{b1} $(b \in \{2, \ldots, B\})$ are i.i.d. zero-mean Gaussian RVs, it is easy to show that S_b is also a Gaussian RV, whose mean and variance are

$$\begin{cases} \mu_{S_b} = 0 \\ \sigma^2_{S_b} = \left(1 + \eta^2\right) \sigma^2_{\text{Shad}} \end{cases}. \tag{6}$$

From the definition of I_b in (5), *the aggregate interference power* in mW from all interfering UEs to the BS of C_1 can be formulated as

$$I^{\text{mW}} = \sum_{b=2}^{B} 10^{\frac{1}{10} I_b}. \tag{7}$$

In our previous work [12], we show that the distribution of I^{mW} can be well approximated by a power lognormal distribution. The results are summarized in the following.

1) The Distribution of $I_b^{(1)}$ in (5): First, we analyze the distribution of $I_b^{(1)}$ shown in (5). With a bounded approximation error in terms of the maximum KS distance [12], [15], we can approximate $I_b^{(1)}$ by a Gaussian RV G_b, whose mean and variance are

$$\begin{cases} \mu_{G_b} = P_0 + \mu_{L_b} + \mu_{S_b} \\ \sigma^2_{G_b} = \sigma^2_{L_b} + \sigma^2_{S_b} \end{cases} \text{(i.e., } P_0 + L_b + S_b \approx G_b), \tag{8}$$

This article has been accepted for publication in a future issue of this journal, but has not been fully edited. Content may change prior to final publication. Citation information: DOI 10.1109/TCOMM.2017.2751552, IEEE Transactions on Communications

Table I: Definition of RVs.

RV notation	Description	PDF
R_b	The coverage area of single-tier small cell C_b	Arbitrary shape and size
Z_b	The position of UE K_b in R_b	$f_{Z_b}(z), z \in R_b$
d_{bm}	The distance (in km) from UE K_b to the BS of small cell C_m	Function of $f_{Z_b}(z)$, R_b and D_b
L_{bm}	The path loss (in dB) from UE K_b to the BS of small cell C_m	Function of $f_{Z_b}(z)$, R_b and D_b
S_{bm}	The shadow fading (in dB) from UE K_b to the BS of small cell C_m	i.i.d. $\mathcal{N}\left(0, \sigma^2_{\text{Shad}}\right)$
H_{bm}	The channel gain (in dB) from UE K_b to the BS of small cell C_m	$f_{H_{bm}}(h)$
P_b	The UL transmission power (in dBm) of UE K_b	Function of $f_{Z_b}(z)$, R_b and S_{bb}

where μ_{L_b} and $\sigma^2_{L_b}$ are respectively the mean and the variance of L_b, which can be obtained using numerical integration involving $f_{Z_b}(z)$ and R_b as [11], [12]

$$\begin{aligned}\mu_{L_b} &= \int_{-\infty}^{+\infty} l f_{L_b}(l)\, dl \\ &= \int_{R_b} L_b(z)\, f_{Z_b}(z)\, dz \\ &= \int_{R_b} \left(\eta L_{bb}(z) - L_{b1}(z)\right) f_{Z_b}(z)\, dz, \end{aligned} \tag{9}$$

$$\begin{aligned}\sigma^2_{L_b} &= \int_{-\infty}^{+\infty} (l-\mu_{L_b})^2 f_{L_b}(l)\, dl \\ &= \int_{R_b} \left(L_b(z) - \mu_{L_b}\right)^2 f_{Z_b}(z)\, dz \\ &= \int_{R_b} \left(\eta L_{bb}(z) - L_{b1}(z) - \mu_{L_b}\right)^2 f_{Z_b}(z)\, dz. \end{aligned} \tag{10}$$

where (1) should be further plugged into (9) and (10) to obtain the numerical results, which take the random UE-to-BS distances into account.

2) The Distribution of I_b in (5): Second, we analyze the distribution of $I_b = I_b^{(1)} + H_{b1}$ shown in (5). With a bounded approximation error in terms of the maximum KS distance [12], [15], we approximate I_b by another Gaussian RV Q_b, whose mean and variance are

$$\begin{cases} \mu_{Q_b} = \mu_{G_b} + \mu_{H_{b1}} \\ \sigma^2_{Q_b} = \sigma^2_{G_b} + \sigma^2_{H_{b1}} \end{cases} \text{(i.e., } G_b + H_{b1} \approx Q_b). \tag{11}$$

where $\mu_{H_{b1}}$ and $\sigma^2_{H_{b1}}$ are respectively the mean and the variance of H_{b1}. According to the RV definition presented in Section III, $\mu_{H_{b1}}$ and $\sigma^2_{H_{b1}}$ can be computed by

$$\mu_{H_{b1}} = \int_{-\infty}^{+\infty} h f_{H_{b1}}(h)\, dh, \tag{12}$$

$$\sigma^2_{H_{b1}} = \int_{-\infty}^{+\infty} (h-\mu_{H_{b1}})^2 f_{H_{b1}}(h)\, dh, \tag{13}$$

where $f_{H_{b1}}(h)$ can be derived according to the distribution of H_{b1} defined in (3).

3) The Distribution of I^{mW} in (7): Third, we invoke the main results in [21], [22], which indicate that the sum of multiple independent lognormal RVs can be well approximated by a power lognormal RV. Thus, in our case, since each $I_b, b \in \{2, \ldots, B\}$, is approximated by a Gaussian RV Q_b, their sum $10^{\frac{1}{10}Q_b}$ in (7) should be well approximated by a power lognormal RV expressed as $\hat{I}^{\text{mW}} = 10^{\frac{1}{10}Q}$, where the PDF and CDF of Q can be written as [21]

$$\begin{cases} \text{PDF of } Q: \\ f_Q(q) = \lambda \left[\Phi\left(\frac{q-\mu_Q}{\sigma_Q}\right)\right]^{\lambda-1} \frac{1}{\sqrt{2\pi\sigma^2_Q}} \exp\left\{-\frac{(q-\mu_Q)^2}{2\sigma^2_Q}\right\} \\ \text{CDF of } Q: \\ F_Q(q) = \left[\Phi\left(\frac{q-\mu_Q}{\sigma_Q}\right)\right]^{\lambda} \end{cases}, \tag{14}$$

where $\Phi(x)$ is the CDF of the standard normal distribution, and the parameters λ, μ_Q and σ_Q are obtained from $\{\mu_{Q_b}\}$ and $\{\sigma^2_{Q_b}\}$ shown in (11). The numerical procedure to obtain λ, μ_Q and σ_Q can be found in [21], [22]. A short summary of such numerical procedure is available in Appendix B of [12]. From (14), the PDF and CDF of $\hat{I}^{\text{mW}}$ can be written as [21]

$$\begin{cases} \text{PDF of } \hat{I}^{\text{mW}}: \\ f_{\hat{I}^{\text{mW}}}(v) = \lambda\left[\Phi\left(\frac{\zeta \ln v - \mu_Q}{\sigma_Q}\right)\right]^{\lambda-1} \frac{\zeta}{v\sqrt{2\pi\sigma^2_Q}} \exp\left\{-\frac{(\zeta \ln v - \mu_Q)^2}{2\sigma^2_Q}\right\} \\ \text{CDF of } \hat{I}^{\text{mW}}: \\ F_{\hat{I}^{\text{mW}}}(v) = \left[\Phi\left(\frac{\zeta \ln v - \mu_Q}{\sigma_Q}\right)\right]^{\lambda} \end{cases}, \tag{15}$$

where $\zeta = \frac{10}{\ln 10}$ is a scalar factor originated from a variable change from $10\log_{10} v$ to $\ln v$.

Finally, we approximate the distribution of I^{mW} by that of $\hat{I}^{\text{mW}}$ shown in (15).

4) The Approximation Errors: The upper bound of the total error of approximating $I_b^{(1)}$ by G_b in Subsection IV-A1 and approximating I_b by Q_b in Subsection IV-A2, is obtained from the summation of the individual approximation errors of the two steps in closed-form expressions [12]. Intuitively speaking, the results in [12] showed that the larger the variance of the Gaussian RV, i.e., S_b in (8) or G_b in (11), the better the approximation in (8) or in (11), due to the increasing dominance of the Gaussian RV. In Appendix A, we provide a toy example to show our previous finding that the sum of a Gaussian RV and an *arbitrary* RV can be well approximated by another Gaussian RV, when the variance of the summand Gaussian RV is larger than that of the summand *arbitrary* RV [12].

Moreover, the bounds of the error of approximating the distribution of I^{mW} by that of $\hat{I}^{\text{mW}}$ in Subsection IV-A3 are still unknown. But it has been shown to be reasonably small in practical cases [21], [22]. In Section V, we will also

This article has been accepted for publication in a future issue of this journal, but has not been fully edited. Content may change prior to final publication. Citation information: DOI 10.1109/TCOMM.2017.2751552, IEEE Transactions on Communications

confirm that the approximation error of the power lognormal distribution is indeed small for the 4G networks defined by the 3GPP.

B. The Signal Power Analysis

Based on the definition of RVs discussed in Section III, *the UL received signal power* in dBm from UE K_1 to its serving BS of C_1 can be written as

$$\begin{aligned} X_1 &\overset{(a)}{=} P_1 - L_{11} - S_{11} + H_{11} \\ &= P_0 + \underbrace{(\eta L_{11} - L_{11})}_{\bar{L}_{11}} + \underbrace{(\eta S_{11} - S_{11})}_{\bar{S}_{11}} + H_{11} \\ &= \underbrace{\left(P_0 + \bar{L}_{11} + \bar{S}_{11}\right)}_{X_1^{(1)}} + H_{11} \\ &= X_1^{(1)} + H_{11}, \end{aligned} \tag{16}$$

where (2) is plugged into the step (a) of (16). Besides, $\bar{L}_{11}$ and $\bar{S}_{11}$ are defined as $\bar{L}_{11} = (\eta - 1) L_{11}$ and $\bar{S}_{11} = (\eta - 1) S_{11}$, respectively. Apparently, $\bar{L}_{11}$ and $\bar{S}_{11}$ are *independent* RVs. The first part of X_1 is further defined as $X_1^{(1)} = P_0 + \bar{L}_{11} + \bar{S}_{11}$, and it is easy to show that $\bar{S}_{11}$ is a Gaussian RV, whose mean and variance are

$$\begin{cases} \mu_{\bar{S}_{11}} = 0 \\ \sigma^2_{\bar{S}_{11}} = (1-\eta)^2 \sigma^2_{\text{Shad}} \end{cases}. \tag{17}$$

Similar to the discussion in Subsection IV-A1, with a bounded approximation error in terms of the maximum KS distance [12], [15], we can approximate $X_1^{(1)}$ by a Gaussian RV G_1, whose mean and variance are

$$\begin{cases} \mu_{G_1} = P_0 + \mu_{\bar{L}_{11}} + \mu_{\bar{S}_{11}} \\ \sigma^2_{G_1} = \sigma^2_{\bar{L}_{11}} + \sigma^2_{\bar{S}_{11}} \end{cases} \left(\text{i.e., } P_0 + \bar{L}_{11} + \bar{S}_{11} \approx G_1\right), \tag{18}$$

where $\mu_{\bar{L}_{11}}$ and $\sigma^2_{\bar{L}_{11}}$ are respectively the mean and the variance of $\bar{L}_{11}$. As a result, (16) can be re-formulated as

$$X_1 \approx G_1 + H_{11} \triangleq \hat{X}_1. \tag{19}$$

Unlike the discussion in Subsection IV-A2, it is questionable to further approximate $\hat{X}_1$ by a Gaussian RV, because the randomness of the Gaussian distributed RV S_{11} is largely removed by the UL transmission power control mechanism, rendering a less dominant role of the Gaussian distribution of G_1 compared with the distribution of H_{11}. Note that the variance of $\bar{S}_{11}$ is as small as $(1-\eta)^2 \sigma^2_{\text{Shad}}$ shown in (17), while that of S_b is as large as $\left(1+\eta^2\right) \sigma^2_{\text{Shad}}$ presented in (6). In other words, $\sigma^2_{G_1} = \sigma^2_{\bar{L}_{11}} + \sigma^2_{\bar{S}_{11}}$ could be comparable with or even smaller than the variance of H_{11}, making the Gaussian approximation error large according to the results in [12]. Hence, our conclusion on $\hat{X}_1$ is presented in Remark 1 as follows.

Remark 1: It is generally *not* accurate to approximate $\hat{X}_1$ in (19) by a Gaussian RV because the Gaussian distribution of G_1 is less dominant than the distribution of H_{11} in terms of the distribution variance.

Note that Remark 1 has been validated by the toy example in Appendix A. In more detail, suppose that H_{11} follows a uniform distribution, we have shown in Fig. 8 that the Gaussian approximation on $(G_1 + H_{11})$ is *not* accurate when the Gaussian distribution of G_1 is less dominant than the distribution of H_{11} in terms of the distribution variance. Since H_{11} might be characterized by any form of distribution and there exists at least one example of uniform distribution that prevents the application of the Gaussian approximation on $(G_1 + H_{11})$, we have thus established Remark 1. Note that we will further verify the correctness of Remark 1 using more numerical results under practical network conditions in later sections.

In light of Remark 1, $\hat{X}_1$ takes the form of a Gaussian RV G_1 plus a RV H_{11} with an arbitrary distribution. Equivalently, the signal power in the linear scale is characterized by a product of two RVs, i.e., a lognormal RV and a RV with an arbitrary distribution. Therefore, we need to derive the distribution of $\hat{X}_1$ and thus the approximate distribution of X_1 using a *different* method. Our main results are presented in Theorem 1 as follows.

Theorem 1. *The approximate CDF of X_1 can be derived as*

$$F_{X_1}(x) \approx F_{\hat{X}_1}(x) \approx \frac{1}{\sqrt{\pi}} \sum_{m=1}^{M_0} w_m F_{H_{11}}\left(x - \left(\sqrt{2}\sigma_{G_1} a_m + \mu_{G_1}\right)\right), \tag{20}$$

where $F_{H_{11}}(h)$ is the CDF of H_{11} defined in (3), σ_{G_1} and μ_{G_1} are obtained from (18), M_0 is the number of terms employed in the Gauss-Hermite numerical integration [16], and the weights $\{w_m\}$ and the abscissas $\{a_m\}$ are tabulated in Table 25.10 of [16].

Proof: See Appendix B. ∎

According to the theory of the Gauss-Hermite numerical integration [16], the numerical integration works with any integrand function and the approximation error associated with the numerical integration is in the order of $\frac{M_0!}{2^{M_0}(2M_0)!}$, which decays very fast as M_0 increases. In practice, M_0 should be chosen as a large enough value to ensure a negligible approximation error. In our numerical results to be shown in later sections, the value of M_0 is set to 30, which makes the approximation error less than 10^{-9}.

Regarding the calculation of $F_{H_{11}}(h)$, since H_{11} represents a logarithm variable change from W_{11}, $F_{H_{11}}(h)$ can be expressed in a general form, which is summarized in Lemma 2.

Lemma 2. *$F_{H_{11}}(h)$ can be written as*

$$F_{H_{11}}(h) = F_{W_{11}}\left(\exp\left(\frac{h}{\zeta}\right)\right), \tag{21}$$

where $F_{W_{11}}(w)$ is the CDF of W_{11} and $\zeta = \frac{10}{\ln 10}$.

Proof: See Appendix C. ∎

Regarding Lemma 2, several special cases can be discussed in the following.

In the case of Rayleigh fading with single-antenna BSs [20], W_{11} follows an exponential distribution with a mean of one, and the CDF of W_{11} can be written as

$$F_{W_{11}}(w) = \Pr[W_{11} \le w] = 1 - \exp(-w). \tag{22}$$

In the case of Rayleigh fading with multi-antenna BSs,

This article has been accepted for publication in a future issue of this journal, but has not been fully edited. Content may change prior to final publication. Citation information: DOI 10.1109/TCOMM.2017.2751552, IEEE Transactions on Communications

W_{11} follows a chi-squared distribution with $2N^{\text{BS}}$ degrees of freedom [20], and the CDF of W_{11} can be written as

$$F_{W_{11}}(w) = \Pr[W_{11} \le w] = \frac{1}{(2N^{\text{BS}}-1)!}\gamma\left(2N^{\text{BS}}, w\right), \quad (23)$$

where $\gamma(\cdot,\cdot)$ denotes the incomplete gamma function [16].

In the case of Nakagami fading with single-antenna BSs, W_{11} follows a Gamma distribution with parameters k and θ [20], and the CDF of W_{11} can be written as

$$F_{W_{11}}(w) = \Pr[W_{11} \le w] = P\left(k, \frac{w}{\theta}\right), \quad (24)$$

where $P(\cdot,\cdot)$ denotes the regularized Gamma function [16], k and θ are the shape and the scale parameters of the Gamma distribution, respectively.

Note that an alternative characterization of the product of lognormal shadow fading and Rayleigh multi-path fading is known as the Suzuki distribution [23]. Compared with [23], the advantage of Theorem 1 roots in its generality, i.e., any form of $F_{W_{11}}(w)$ can be plugged into Lemma 2 and Theorem 1 to obtain an approximate distribution of the signal power.

C. The SIR Analysis

From (16), we can approximate the UL SIR in dB unit by

$$U^{\text{dB}} \approx X_1 - Q \triangleq \hat{U}^{\text{dB}}. \quad (25)$$

Equivalently, the UL SIR in the linear scale takes the form of $\frac{\text{a lognormal RV} \times \text{an arbitrary RV}}{\text{a power lognormal RV}}$. In the following, we derive the approximate distribution of U^{dB} in Theorem 3.

Theorem 3. *The approximate CDF of U^{dB} can be derived as* $F_{U^{dB}}(u) \approx F_{\hat{U}^{dB}}(u)$

$$\approx \frac{\lambda}{\sqrt{\pi}}\sum_{m=1}^{M_0} w_m \Phi^{\lambda-1}\left(\sqrt{2}a_m\right) F_{X_1}\left(u + \sqrt{2}\sigma_Q a_m + \mu_Q\right), \quad (26)$$

where $F_{X_1}(x)$ is the CDF of X_1 computed from Theorem 1, $\{\lambda, \sigma_Q, \mu_Q\}$ are defined in (14), M_0 is the number of terms employed in the Gauss-Hermite numerical integration [16], and the weights $\{w_m\}$ and the abscissas $\{a_m\}$ are tabulated in Table 25.10 in [16].

Proof: See Appendix D. ∎

Corresponding to the special cases discussed for Theorem 1 and Lemma 2, the SIR results can be obtained from Theorem 3 for Rayleigh/Nakagami fading with single-antenna/multi-antenna BSs, respectively.

The complexity of computing $F_{U^{\text{dB}}}(u)$ in Theorem 3 is analyzed as follows:

- w_m and $\Phi\left(\sqrt{2}a_m\right)$ can be readily obtained from the weights and the abscissas of the Gauss-Hermite numerical integration [16], and hence their complexity can be ignored.
- λ, μ_Q and σ_Q need to be calculated for only once and can be used for all values of m and z. The key step to compute λ, μ_Q and σ_Q is to obtain $\{\mu_{Q_b}\}$ and $\{\sigma^2_{Q_b}\}$ shown in (11), and most computations associated with this step are caused by the numerical integration in (9) and (10). More specifically, suppose that $f_{Z_b}(z)$ is sampled by N^{intg} points, then the complexity of calculating λ, μ_Q and σ_Q is in the order of $2BN^{\text{intg}}$.
- $F_{X_1}\left(u + \sqrt{2}\sigma_Q a_m + \mu_Q\right)$ needs to be evaluated for each m and its complexity is in the order of M_0 according to Theorem 1. Hence, for a given u, the complexity associated with the computation of $F_{X_1}\left(u + \sqrt{2}\sigma_Q a_m + \mu_Q\right)$ is in the order of M_0^2.
- To sum up, the complexity of computing $F_{U^{\text{dB}}}(u)$ is in the order of $2BN^{\text{intg}} + M_0^2$, which is feasible in practice considering that the typical values of B, N^{intg} and M_0 are in the order of several tens to hundreds.

Furthermore, regarding Theorem 3, we have two remarks in the following.

Remark 2: Since Theorem 3 is built upon (9) and (10), which poses no constraints on R_b and $f_{Z_b}(z)$, the DNA-GA analysis can handle arbitrary UE distributions.

Remark 3: Even if $f_{Z_b}(z)$ is constant over z, we can only say that the UE distribution is uniform within the small cell coverage area R_b, as illustrated in Fig. 1d. However, from Fig. 1d, it is clear that the UE distribution is *not* uniform within the entire network area, because no UE is deployed outside the hotspot areas $\{R_b\}$, and consequently the UE distribution within the entire network area is *not* uniform. Note that in the macroscopic analysis based on stochastic geometry [5], [6], UEs are usually assumed to be Poisson-distributed within the entire network area as illustrated in Fig. 1b. In the sequel, the description of the UE distribution is meant within R_b since we are focusing on the microscopic analysis. For example, a uniform UE distribution means that UEs are uniformly deployed in $\{R_b\}$, *not* in the entire network area.

D. Special Use Cases of the DNA-GA Analysis

With Theorem 3, we have crafted a new microscopic analysis based on the proposed DNA-GA analysis, which can deal with a wide range of network assumptions, UE and BS distributions, and system parameters. In this section, we discussed two special network scenarios of the proposed DNA-GA analysis.

1) The Grid Network Scenario: A typical network scenario widely used in the microscopic analysis is *the grid network scenario* [5]. Such network scenario is referred to as NS 3 in Section I and illustrated by Fig. 1c. More specifically, we construct an idealistic BS deployment on a perfect hexagonal lattice, and then we can perform a single DNA-GA analysis on such BS deployment to extract an upper-bound of the SIR performance. Note that the BS deployment on a hexagonal lattice leads to an upper-bound performance, because BSs are evenly distributed in the network scenario, and thus very strong interference due to close proximity is precluded in the analysis [5], [6].

2) The Random Deployment Network Scenario: Instead of using the grid network case, we can choose a specific network scenario with *random BS deployment* and apply the DNA-GA analysis on it. Such network scenario is referred to as NS 4 in Section I and illustrated by Fig. 1d. However, such practice might lead to a biased judgment on the quality of the DNA-GA analysis, since unlike the deterministic grid network scenario

This article has been accepted for publication in a future issue of this journal, but has not been fully edited. Content may change prior to final publication. Citation information: DOI 10.1109/TCOMM.2017.2751552, IEEE Transactions on Communications

in Subsection IV-D1, the choice of a specific network scenario is a highly subjective one. Hence, it might be better to apply the DNA-GA analysis, i.e., Theorem 3, over N^{dep} random BS deployments and obtain the average performance result, e.g., averaging over N^{dep} CDFs to obtain an average CDF.

V. Simulation and Discussion

In this section, we conduct simulations to validate the proposed DNA-GA analysis, using both NS 3 and NS 4:

- For NS 3, only *one* BS deployment on a hexagonal lattice is examined.
- For NS 4, we *average* the results given by Theorem 3 over *1000* random BS deployments.

For each BS deployment, *10,000* random experiments are conducted to go through the randomness of UE positions, and for each BS deployment and each UE placement, another *10,000* random experiments are conducted to go through the randomness of shadow fading and multi-path fading. M_0 is set to 30 for the computation in the DNA-GA analysis to ensure a good accuracy of the results [16]. Note that the the scale of simulations seems to be very large in our work. More specifically, in our simulations involving 228 small cells, the following sets of random variables (RVs) should be considered for each random BS deployment:

- Set 1: 228 two-dimensional RVs associated with random UE distribution
- Set 2: 228 RVs associated with shadow fading for the active UEs
- Set 3: $228 \times N^{\text{BS}}$ RVs associated with multi-path fading for the active UEs, where N^{BS} denotes the antenna number at BSs

In our simulations, we conducted *10,000* experiments to investigate the randomness of the RVs in Set 1, which contains 456 effective RVs. In addition, we conducted another *10,000* experiments to study the randomness of the RVs in Set 2 and Set 3, which also contains at least 456 effective RVs. Our target was to have $10000/456 \approx 20$ tries per RV, which seemed to be reasonable in simulation experiments. However, even with such moderate target, the simulation had already become exceptionally computation-intensive and time-consuming because its complexity is in the order of hundreds of millions. On the other hand, the complexity of evaluating Theorem 3 is in the order of tens of thousands, as discussed before.

With regard to the network parameters, the 3GPP recommendations have been used [18]. For NS 4, 19 dummy macrocell sites are deployed with a 0.5 km inter-site distance to guide the small cell deployment. Each macrocell site has the shape of a hexagon, and is equally divided into 3 pentagon-shaped macrocells. Each macrocell contains 4 randomly deployed small cells, resulting in $19 \times 3 \times 4 = 228$ small cells with a density around 55.43 cells/km^2. For NS 3, the 228 small cells are located on a hexagonal lattice with the same cell density. In both cases, each small cell has a coverage radius of 0.04 km as recommended by the 3GPP to simulate a hotspot with a small cell BS at the center of it, and the minimum inter-BS distance and the minimum BS-to-UE distance are 0.04 km, and 0.01 km, respectively. Moreover, according to [18], we use the following parameters $A = 145.4$, $\alpha = 3.75$, $P_0 = -76$ dBm, $\eta = 0.8$, and $\sigma_S = 10$ dB.

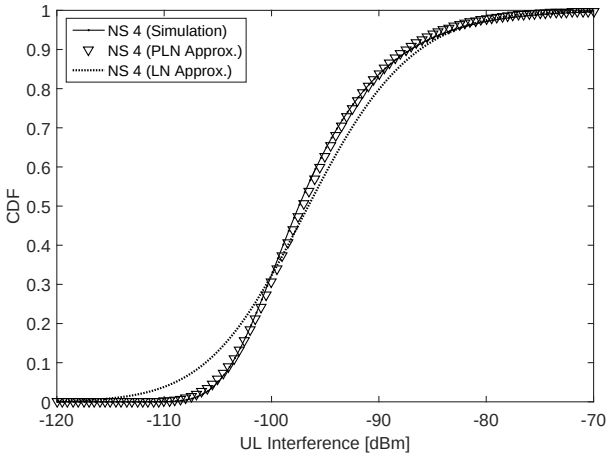

Fig. 3: The UL aggregate interference power in dBm (Case 1). Note that in this figure, LA and PLA represent Lognormal Approximation [24] and Power Lognormal Approximation [12], respectively.

In the following subsections, we will validate the accuracy of the DNA-GA analysis in terms of the interference power, the signal power and the SIR performance.

A. Validation of the DNA-GA Analysis

In this subsection, we validate the accuracy of the DNA-GA analysis using NS 4 together with the following case,

- **Case 1:** uniform UE distribution + Rayleigh fading + single-antenna BSs

Note that NS 4 is chosen because it represents numerous network realizations, instead of just one network scenario as in NS 3.

1) Validation of the Interference Power: In Fig. 3, we show the UL aggregate interference power averaged over *1000* random BS deployments. As concluded in our previous work [12], the UL aggregate interference power can be well approximated by a power lognormal distribution. Specifically, in Fig. 3, the maximum deviation in terms of the maximum KS distance between the simulated CDF and the power lognormal CDF obtained by our analysis is less than 1.9 percentile, which validates the accuracy of the first part of the DNA-GA analysis presented in Subsection IV-A. The previous state-of-the-art conclusion was that the UL aggregate interference should be approximated by a lognormal RV [24]. For completeness, we also show such lognormal approximation in Fig. 3 and we can see that it is much less accurate than the approximation using the proposed power lognormal distribution [12].

2) Validation of the Signal Power: For Case 1, we obtain the signal power from the DNA-GA analysis using Theorem 1. In Fig. 4, we plot such UL signal power averaged over *1000* random BS deployments. As discussed in Remark 1 and shown in Fig. 4, it is indeed *not* accurate to approximate the dB-scale UL signal power by a Gaussian RV, because the randomness of the Gaussian distributed shadow fading is largely mitigated

This article has been accepted for publication in a future issue of this journal, but has not been fully edited. Content may change prior to final publication. Citation information: DOI 10.1109/TCOMM.2017.2751552, IEEE Transactions on Communications

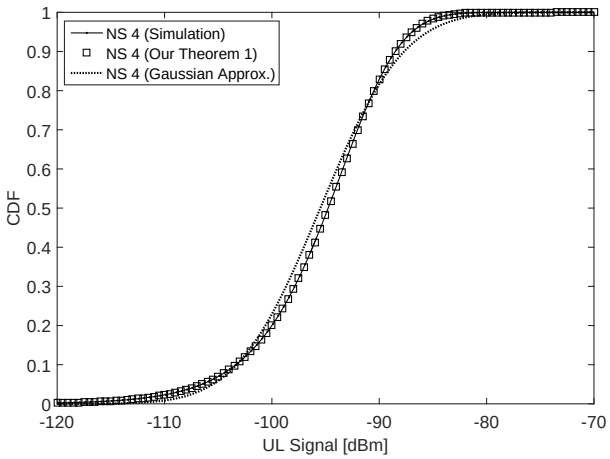

Fig. 4: The UL signal power in dBm (Case 1). Note that in this figure, the directly Gaussian approximation [12] is *not* accurate for the signal power.

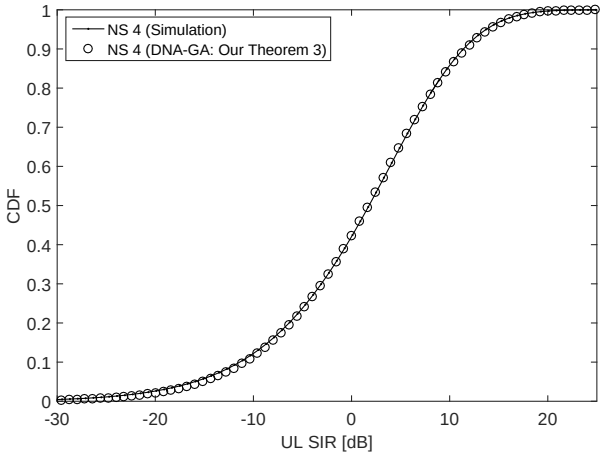

Fig. 5: The UL SIR in dB (Case 1).

by the considered UL transmission power control mechanism. From Fig. 4, we can see that the proposed Theorem 1 gives a good approximation of the UL signal power, which validates the accuracy of the second part of the DNA-GA analysis presented in Subsection IV-B. More specifically, in Fig. 4, the maximum deviation in terms of the maximum KS distance between the simulated CDF and the analytical CDF using Theorem 1 is less than 0.2 percentile.

3) Validation of the SIR: After confirming the accuracy of the distributions for the aggregate interference power and the signal power, we can obtain the average SIR results for Case 1 over *1000* random BS deployments using the DNA-GA analysis addressed in Theorem 3. In Fig. 5, we plot such UL SIR in dB unit. From this figure, we can see that the results given by the DNA-GA analysis match well with the simulation results, which validates the accuracy of the third part of the DNA-GA analysis presented in Subsection IV-C. In more detail, in Fig. 5, the maximum deviation in terms of the maximum KS distance between the simulated CDF and the analytical CDF using Theorem 1 is less than 0.7 percentile.

It is very important to note that in Fig. 5 the curve-matching of the average results over *1000* random BS deployments does

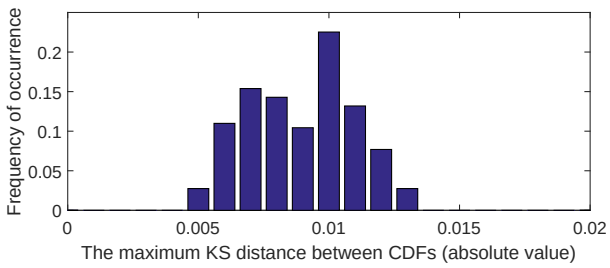

Fig. 6: The frequency of occurrence of the maximum KS distance between the simulated CDF and the analytical CDF (Case 1).

not necessarily mean that the approximated CDF matches the simulated CDF for *each* BS deployment. To investigate the accuracy of the DNA-GA analysis for *each* BS deployment, we plot the frequency of occurrence of the maximum KS distance between the simulated CDF and the analytical CDF in Fig. 6. From this figure, we can observe that for around 90% BS deployments, the approximation errors are less than 1.1 percentile, which is a bit larger than the error shown in Fig. 5 since a negative error and a positive error may cancel each other out in the average operation over *1000* random BS deployments. Overall, such per-BS-deployment approximation error shows that the DNA-GA analysis is good enough for practical usage since it merely incurs a small error around 1 percentile.

B. Investigation of Alternative Scenarios

With the DNA-GA analysis validated in Subsection V-A, in this subsection, we investigate the results of the DNA-GA analysis for alternative cases compared against Case 1 to show the generality of our analysis. The additional cases are defined as follows,

- **Case 2:** non-uniform UE distribution + Nakagami fading + single-antenna BSs
- **Case 3:** uniform UE distribution + Rayleigh fading + multi-antenna BSs ($N^{\mathrm{BS}} = 4$)

When considering a non-uniform UE distribution in Case 2, we assume that $f_{Z_b}(z) = \frac{W}{\rho}, z \in R_b$, where ρ is the radial coordinate of z in the polar coordinate system, the origin of which is placed at the position of the BS of C_b and W is a normalization constant to make $\int_{R_b} f_{Z_b}(z)\, dz = 1$. In the resulting non-uniform UE distribution, UEs are more likely to locate in the close vicinity of the BS of C_b than at the cell-edge. Note that the considered $f_{Z_b}(z)$ is just an example of the non-uniformly distributed UEs in R_b, which reflects a reasonable network planning, where small cell BSs have been deployed at the center of UE clusters. Other forms of $f_{Z_b}(z)$ can be considered in our DNA-GA analysis as well.

When considering Nakagami fading in Case 2, we assume that $k = 10$ and $\theta = 0.1$, which corresponds to a multi-path fading with a strong line-of-sight (LoS) component [20]. Note that Case 2 is just an example for performance evaluation. Other values of k and θ can be considered in our DNA-GA analysis as well.

This article has been accepted for publication in a future issue of this journal, but has not been fully edited. Content may change prior to final publication. Citation information: DOI 10.1109/TCOMM.2017.2751552, IEEE Transactions on Communications

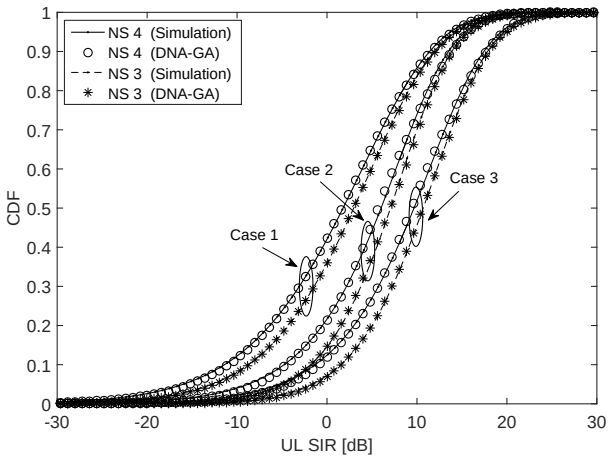

Fig. 7: UL SIR in dB with the DNA-GA analysis vs. the simulation (various cases). Note that the analytical upper-bound performance is obtained using NS 3 as illustrated in Fig. 1c.

For all of the interested cases, the average UL SIR performance is evaluated for NS 4 as discussed in Subsection IV-D2. Moreover, the upper bound of the UL SIR is investigated for NS 3 as discussed in Subsection IV-D1.

The SIR results are shown in Fig. 7. As can be seen from this figure, the SIR results of the proposed DNA-GA analysis match well with those obtained by simulation. For NS 4, the maximum deviation in terms of the maximum KS distance between the CDFs obtained by the DNA-GA analysis and the simulation for all of the investigated cases are around $0.9 \sim 1.7$ percentile. For NS 3, the fitness becomes even better, i.e., the maximum deviation in terms of the maximum KS distance for all of the investigated scenarios is within 0.6 percentile.

More importantly, for all of the investigated cases, the upper-bound SIR performance given by NS 3 is shown to be within $2.0 \sim 2.5$ dB from the average performance obtained from NS 4, indicating its usefulness in characterizing the network performance with low-complexity computation. In more detail, the numerical results to be plugged into Theorem 3 to obtain the upper-bound SIR performance for the grid network scenario shown in Fig. 1c are as follows,

- Case 1: $\mu_{G_1} = -93.07$, $\sigma^2_{G_1} = 5.97$, $\lambda = 202.66$, $\mu_Q = -137.71$ and $\sigma^2_Q = 212.04$.
- Case 2: $\mu_{G_1} = -92.30$, $\sigma^2_{G_1} = 7.15$, $\lambda = 193.48$, $\mu_Q = -137.01$ and $\sigma^2_Q = 193.66$.
- Case 3: The same as Case 1, because Case 1 and Case 3 share the same G_1 and Q. However, $F_{H_{11}}(h)$ is different for Case 1 and Case 3, which leads to different $F_{Z^{\text{dB}}}(z)$.

Finally, note that the SIR of Case 2 outperforms that of Case 1, mainly because UEs tend to stay closer to their serving BSs in the considered non-uniform UE distribution of Case 2, leading to a larger signal power and a lower interference power. Also note that Case 3 achieves the best SIR performance among the interested cases due to the MRC antenna array gain provided by the multi-antenna BSs.

C. The Application and Future Work of the DNA-GA Analysis

The proposed DNA-GA analysis based on the Gaussian approximation is particularly useful for network performance analysis of the 5G systems with general cell deployment and user distribution. Detailed discussion is provided in the following.

- The Gaussian approximation has been shown to be more accurate for denser and smaller cells [11], [12], because the Gaussian distribution originated from the shadow fading becomes more dominant compared with the random UE distribution in each cell of a denser SCN.
- The Gaussian approximation can be applied to cell coverage areas with arbitrary shapes. This is very useful to analyze 5G hotspots with irregular shapes, as illustrated in Fig. 1b.
- The Gaussian approximation becomes strongly motivated in response to the emerging issue of fast shadow fading in 5G. This issue is brought forth by a recent significant discovery that the 5G network capacity will decrease to *zero* if the antenna height difference between BSs and UEs is *non-zero* [25]–[27]. A simple solution to avoid such network crash is to lower the BS antenna height to the UE height around 1.5 m. However, such BS deployment gives rise to a new issue of fast shadow fading caused by moving vehicles on streets with a similar height of 1.5 m. In more detail, considering a typical car length of 4 m and a moderate vehicle speed of 36 km/h, the time interval that such vehicle blocks a communication link becomes 400 ms, which leads to a new phenomenon of fast shadow fading. Note that a larger vehicle speed would result in an even faster shadow fading. Such fast shadow fading issue was highlighted by the International Telecommunication Union (ITU) document considering trees and moving vehicles in [28]. It was not a real concern until recently when we are marching toward 5G and continuously lowering the BS antennas below tree lines. With the existence of the fast shadow fading, the Gaussian distribution will become more dominant for each UE-to-BS link, making the Gaussian approximation more useful in analyzing network performance in the future.
- The Gaussian approximation is capable of generating results for operators who want to know *the performance of a specific BS deployment in its network or the performance impact of adding several specific BSs to its network*. This is because the Gaussian approximation is naturally applied on each specific BS, and thus providing a microscopic treatment of 5G SCNs to identify network deployment problems or verify incremental network upgrade plans for operators.

As future work, the proposed DNA-GA analysis can be enhanced in several aspects. Detailed discussion is provided in the following.

- The proposed DNA-GA analysis based on the Gaussian approximation is complimentary to the stochastic geometry analysis [5], [6]. They are both useful for network performance analysis in 5G. In particular, the stochastic

This article has been accepted for publication in a future issue of this journal, but has not been fully edited. Content may change prior to final publication. Citation information: DOI 10.1109/TCOMM.2017.2751552, IEEE Transactions on Communications

geometry analysis investigates average results, while the DNA-GA analysis reveals more detailed results for specific network deployments. Note that the BS density in the stochastic geometry analysis is usually assumed to be a Poisson distributed RV. Hence, using the DNA-GA analysis to obtain comparable results as in the stochastic geometry analysis would be highly inefficient, and hence a direct comparison between these two analyses is not very meaningful for now. However, it would be very interesting to investigate whether there exists a way to upgrade the DNA-GA analysis to a macroscopic analysis tool, and then make a fair comparison between the DNA-GA analysis and the stochastic geometry analysis.

- The proposed DNA-GA analysis handles homogeneous SCNs very well. However, it needs further study on the feasibility of applying the DNA-GA analysis to the co-channel HetNet scenario discussed in Section I. Note that the Gaussian approximation was shown to be less accurate for sparse macrocells [11], [12], because the Gaussian distribution originated from the shadow fading becomes less dominant compared with the random UE distribution. Hence, for the treatment of the co-channel HetNet scenario, it would be interesting to enhance the DNA-GA analysis considering the techniques in [29], [30].
- It needs further study on the impact of correlated shadow fading [19] on the proposed DNA-GA analysis. Note that in this case, the UL interference distributions become correlated. Besides, it needs further study on the feasibility of applying the proposed DNA-GA analysis to the downlink (DL) SCNs. Note that for the DL case, the signal power and the interference power become correlated, e.g., a cell edge UE in the DL tends to have a lower signal power and a higher interference power, while in the UL the interference power is independently distributed with respect to the signal power.
- The proposed DNA-GA analysis ignores the maximum power constraint, which is shown by (2). However, this should not limit the generality of the DNA-GA framework. It needs further study on how the interference distribution should be modified if we consider the maximum power constraint. Note that the DNA-GA analysis might be benefited from several new techniques, in which uplink power control with maximum power constraint can be tackled [31], [32].

VI. Conclusion

We propose a tractable semi-analytical approach of network performance analysis, i.e., the DNA-GA analysis, which is capable of handling lognormal shadow fading, any shape and/or size of cell coverage areas, any UE distribution, any type of multi-path fading, and multi-antenna BSs. Thus, the DNA-GA analysis can evaluate many realistic networks and is useful for the network performance analysis of the 5G systems with general cell deployment and UE distribution.

Appendix A: On the Gaussian Approximation

Suppose that a zero-mean RV $\tilde{G}$ is a sum of two independent RVs, i.e., a zero-mean *arbit*rary RV $\tilde{L}$ and a zero-mean Gaussian RV $\tilde{S}$. More specifically, we have $\tilde{G} = \tilde{L} + \tilde{S}$. The Gaussian approximation approach is to approximate $\tilde{G}$ by a another Gaussian RV $\tilde{Y}$ with a variance of $\left(\sigma_L^2 + \sigma_S^2\right)$, where σ_L^2 and σ_S^2 are the variances of $\tilde{L}$ and $\tilde{S}$, respectively. In order to quantify the approximation error between the distribution of $\tilde{G}$ and its approximate Gaussian distribution of $\tilde{Y}$, in [12] we invoke the definition of the Kolmogorov–Smirnov (KS) distance between two CDFs [15], which is a widely used metric to measure the difference between two CDFs by showing the maximum absolute error over all the possible RV values. In essence, the theorem in [12] stated that the sum of a Gaussian RV and an *arbitrary* RV can be well approximated by another Gaussian RV, when the variance of the summand Gaussian RV is larger than or comparable to that of the summand *arbitrary* RV.

Toy Example: Suppose that $\sigma_S = 5$, and the summand *arbitrary* RV $\tilde{L}$ follows a uniform distribution with $\sigma_L = \{2, 5, 8\}$. Both RVs are of zero-mean and the CDF of the sum of the two RVs is plotted in Fig. 8.

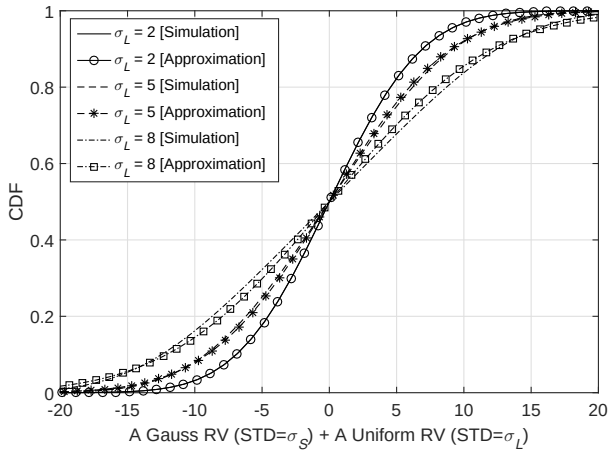

Fig. 8: The CDF of the sum of a Gaussian RV and a RV with a uniform distribution.

From this figure, we can see that the approximation error associated with the Gaussian approximation is indeed very small when $\sigma_L \leq \sigma_S$. However, such error is non-negligible when $\sigma_L > \sigma_S$. More specifically, we can quantify the actual CDF error as 6.16×10^{-4}, 1.04×10^{-2} and 2.57×10^{-2} when $\sigma_L = 2$, $\sigma_L = 5$ and $\sigma_L = 8$, respectively. The above results confirm the tightness of the approximation and the intuition in [12] that the Gaussian approximation error reduces, as the variance of the summand *arbitrary* RV $\tilde{L}$ decreases, or equivalently the variance of the Gaussian RV $\tilde{S}$ increases.

Appendix B: Proof of Theorem 1

Since G_1 is a Gaussian RV with the mean and the variance shown in (18), the PDF of G_1 can be written as

$$f_{G_1}(v) = \frac{1}{\sqrt{2\pi\sigma_{G_1}^2}} \exp\left\{-\frac{(v-\mu_{G_1})^2}{2\sigma_{G_1}^2}\right\}. \qquad (27)$$

This article has been accepted for publication in a future issue of this journal, but has not been fully edited. Content may change prior to final publication. Citation information: DOI 10.1109/TCOMM.2017.2751552, IEEE Transactions on Communications

Besides, according to the definition of RVs in Section III, we assume the CDF of H_{11} to be $F_{H_{11}}(h)$. Hence, the CDF of X_1 can be approximated by

$$\begin{aligned}
&F_{X_1}(x)\\
&\approx F_{\hat{X}_1}(x)\\
&= \Pr[G_1 + H_{11} \le x]\\
&= \int_{-\infty}^{+\infty} F_{H_{11}}(x-v)\, f_{G_1}(v)\, dv\\
&\overset{(a)}{=} \int_{-\infty}^{+\infty} F_{H_{11}}(x-v)\, \frac{1}{\sqrt{2\pi\sigma_{G_1}^2}} \exp\left\{-\frac{(v-\mu_{G_1})^2}{2\sigma_{G_1}^2}\right\} dv\\
&\overset{(b)}{=} \frac{1}{\sqrt{\pi}} \int_{-\infty}^{+\infty} F_{H_{11}}\left(x - \left(\sqrt{2}\sigma_{G_1} y + \mu_{G_1}\right)\right) \exp\left(-y^2\right) dy\\
&\overset{(c)}{=} \frac{1}{\sqrt{\pi}} \sum_{m=1}^{M_0} w_m F_{H_{11}}\left(x - \left(\sqrt{2}\sigma_{G_1} a_m + \mu_{G_1}\right)\right) + R_{M_0}\\
&\overset{(d)}{\approx} \frac{1}{\sqrt{\pi}} \sum_{m=1}^{M_0} w_m F_{H_{11}}\left(x - \left(\sqrt{2}\sigma_{G_1} a_m + \mu_{G_1}\right)\right), \qquad (28)
\end{aligned}$$

where

- (a) of (28) is obtained from (27),
- (b) of (28) is computed using an exchange of variable: $v = \sqrt{2}\sigma_{G_1} y + \mu_{G_1}$,
- (c) of (28) is derived using the Gauss-Hermite numerical integration [16], i.e.,

$$\int_{-\infty}^{+\infty} f(y) \exp\left(-y^2\right) dy = \sum_{m=1}^{M_0} w_m f(a_m) + R_{M_0}, \quad (29)$$

  where M_0 is the number of terms in the approximation, the weights $\{w_m\}$ and the abscissas $\{a_m\}$ are tabulated in Table 25.10 of [16] and R_{M_0} is a residual error in the order of $\frac{M_0!}{2^{M_0}(2M_0)!}$ [16], which decays very fast as M_0 increases,
- (d) of (28) is obtained by the residual error dropping R_{M_0}.

Our proof is thus completed by comparing (28) and (20) in Theorem 1.

Appendix C: Proof of Lemma 2

As discussed in Section III, the connection between W_{11} and H_{11} is the variable change $H_{11} = 10\log_{10} W_{11}$ defined in (3). Thus, we have

$$\begin{aligned}
F_{H_{11}}(h) &= \Pr[H_{11} \le h]\\
&= \Pr[10\log_{10} W_{11} \le h]\\
&= \Pr\left[\ln W_{11} \le \frac{h}{\zeta}\right]\\
&= \Pr\left[W_{11} \le \exp\left(\frac{h}{\zeta}\right)\right], \qquad (30)
\end{aligned}$$

where $\zeta = \frac{10}{\ln 10}$. Our proof is completed.

Appendix D: Proof of Theorem 3

From (25), the approximate CDF of Z^{dB} can be derived as

$$\begin{aligned}
&F_{Z^{\text{dB}}}(z)\\
&\approx F_{\hat{Z}^{\text{dB}}}(z)\\
&= \Pr[X_1 - Q \le z]\\
&= \int_{-\infty}^{+\infty} F_{X_1}(z+q)\, f_Q(q)\, dq\\
&\overset{(a)}{\approx} \int_{-\infty}^{+\infty} F_{\hat{X}_1}(z+q)\, \lambda\Phi^{\lambda-1}\left(\frac{q-\mu_Q}{\sigma_Q}\right) \frac{1}{\sqrt{2\pi\sigma_Q^2}} \exp\left\{-\frac{(q-\mu_Q)^2}{2\sigma_Q^2}\right\} dq\\
&\overset{(b)}{=} \frac{1}{\sqrt{\pi}} \int_{-\infty}^{+\infty} F_{\hat{X}_1}\left(z + \sqrt{2}\sigma_Q y + \mu_Q\right) \lambda\Phi^{\lambda-1}\left(\sqrt{2}y\right) \exp\left(-y^2\right) dy\\
&\overset{(c)}{=} \frac{1}{\sqrt{\pi}} \sum_{m=1}^{M_0} w_m F_{\hat{X}_1}\left(z + \sqrt{2}\sigma_Q a_m + \mu_Q\right) \lambda\Phi^{\lambda-1}\left(\sqrt{2}a_m\right) + R_{M_0}\\
&\overset{(d)}{\approx} \frac{\lambda}{\sqrt{\pi}} \sum_{m=1}^{M_0} w_m \Phi^{\lambda-1}\left(\sqrt{2}a_m\right) F_{\hat{X}_1}\left(z + \sqrt{2}\sigma_Q a_m + \mu_Q\right), \qquad (31)
\end{aligned}$$

where

- (a) of (31) is calculated using Theorem 1 and (14),
- (b) of (31) is computed using a variable change $q = \sqrt{2}\sigma_Q y + \mu_Q$,
- (c) of (31) is derived using the Gauss-Hermite numerical integration [16] shown in (29),
- (d) of (31) is obtained by dropping the residual error R_{M_0} in the Gauss-Hermite numerical integration [16].

Our proof is thus completed by comparing (31) and (26) in Theorem 3.

References

[1] ArrayComm & William Webb, Ofcom, London, U.K., 2007.

[2] D. López-Pérez, M. Ding, H. Claussen, and A. Jafari, "Towards 1 Gbps/UE in cellular systems: Understanding ultra-dense small cell deployments," *IEEE Communications Surveys Tutorials*, vol. 17, no. 4, pp. 2078–2101, Jun. 2015.

[3] 3GPP, "TR 36.872: Small cell enhancements for E-UTRA and E-UTRAN - Physical layer aspects," Dec. 2013.

[4] D. Lopez-Perez, I. Guvenc, G. de la Roche, M. Kountouris, T. Q. S. Quek, and J. Zhang, "Enhanced intercell interference coordination challenges in heterogeneous networks," *IEEE Wireless Communications*, vol. 18, no. 3, pp. 22–30, Jun. 2011.

[5] J. Andrews, F. Baccelli, and R. Ganti, "A tractable approach to coverage and rate in cellular networks," *IEEE Transactions on Communications*, vol. 59, no. 11, pp. 3122–3134, Nov. 2011.

[6] T. D. Novlan, H. S. Dhillon, and J. G. Andrews, "Analytical modeling of uplink cellular networks," *IEEE Transactions on Wireless Communications*, vol. 12, no. 6, pp. 2669–2679, Jun. 2013.

[7] Y. Zhu, J. Xu, Z. Hu, J. Wang, and Y. Yang, "Distribution of uplink inter-cell interference in OFDMA networks with power control," *2014 IEEE International Conference on Communications (ICC)*, pp. 5729–5734, Jun. 2014.

[8] H. Tabassum, F. Yilmaz, Z. Dawy, and M. S. Alouini, "A framework for uplink intercell interference modeling with channel-based scheduling," *IEEE Transactions on Wireless Communications*, vol. 12, no. 1, pp. 206–217, Jan. 2013.

[9] S. Singh, N. B. Mehta, A. F. Molisch, and A. Mukhopadhyay, "Moment-matched lognormal modeling of uplink interference with power control and cell selection," *IEEE Transactions on Wireless Communications*, vol. 9, no. 3, pp. 932–938, Mar. 2010.

This article has been accepted for publication in a future issue of this journal, but has not been fully edited. Content may change prior to final publication. Citation information: DOI 10.1109/TCOMM.2017.2751552, IEEE Transactions on Communications

[10] J. He, Z. Tang, H. H. Chen, and W. Cheng, "Statistical model of OFDMA cellular networks uplink interference using lognormal distribution," *IEEE Wireless Communications Letters*, vol. 2, no. 5, pp. 575–578, Oct. 2013.

[11] M. Ding, D. López-Pérez, G. Mao, and Z. Lin, "Approximation of uplink inter-cell interference in FDMA small cell networks," *2015 IEEE Global Communications Conference (GLOBECOM)*, pp. 1–7, Dec. 2015.

[12] ——, "Microscopic analysis of the uplink interference in FDMA small cell networks," *IEEE Trans. on Wireless Communications*, vol. 15, no. 6, pp. 4277–4291, Jun. 2016.

[13] M. Ding, D. López-Pérez, A. V. Vasilakos, and W. Chen, "Dynamic TDD transmissions in homogeneous small cell networks," *2014 IEEE International Conference on Communications Workshops (ICC)*, pp. 616–621, Jun. 2014.

[14] ——, "Analysis on the SINR performance of dynamic TDD in homogeneous small cell networks," *2014 IEEE Global Communications Conference*, pp. 1552–1558, Dec. 2014.

[15] F. J. M. Jr., "The Kolmogorov-Smirnov test for goodness of fit," *Journal of the American Statistical Association*, vol. 46, no. 253, pp. 68–78, 1951.

[16] M. Abramowitz and I. Stegun, *Handbook of mathematical functions with formulas, graphs, and mathematical tables (Nineth Ed.)*. Dover, 1972.

[17] M. Ding, D. López-Pérez, G. Mao, and Z. Lin, "DNA-GA: A new approach of network performance analysis," *2016 IEEE International Conference on Communications (ICC)*, pp. 1–7, May 2016.

[18] 3GPP, "TR 36.828: Further enhancements to LTE Time Division Duplex for Downlink-Uplink interference management and traffic adaptation," Jun. 2012.

[19] M. Ding, M. Zhang, D. López-Pérez, and H. Claussen, "Correlated shadow fading for cellular network system-level simulations with wrap-around," *2015 IEEE International Conference on Communications (ICC)*, pp. 2245–2250, Jun. 2015.

[20] J. G. Proakis, *Digital Communications (4th Ed.)*. New York: McGraw-Hill, 2000.

[21] Z. Liu, J. Almhana, and R. McGorman, "Approximating lognormal sum distributions with power lognormal distributions," *IEEE Transactions on Vehicular Technology*, vol. 57, no. 4, pp. 2611–2617, Jul. 2008.

[22] S. S. Szyszkowicz and H. Yanikomeroglu, "Fitting the modified-power-lognormal to the sum of independent lognormals distribution," *Global Telecommunications Conference, 2009. GLOBECOM 2009. IEEE*, pp. 1–6, Nov. 2009.

[23] H. Suzuki, "A statistical model for urban radio propagation," *IEEE Transactions on Communications*, vol. 25, no. 7, pp. 673–680, Jul. 1977.

[24] N. B. Mehta, J. Wu, A. F. Molisch, and J. Zhang, "Approximating a sum of random variables with a lognormal," *IEEE Transactions on Wireless Communications*, vol. 6, no. 7, pp. 2690–2699, Jul. 2007.

[25] M. Ding and D. López-Pérez, "Please Lower Small Cell Antenna Heights in 5G," *IEEE Globecom 2016*, pp. 1–6, Dec. 2016.

[26] ——, "On the performance of practical ultra-dense networks: The major and minor factors," *The IEEE Workshop on Spatial Stochastic Models for Wireless Networks (SpaSWiN) 2017*, pp. 1–8, May 2017. [Online]. Available: https://arxiv.org/abs/1701.07964

[27] A. AlAmmouri, J. G. Andrews, and F. Baccelli, "SINR and throughput of dense cellular networks with stretched exponential path loss," *arXiv:1703.08246 [cs.IT]*, Mar. 2017. [Online]. Available: http://arxiv.org/abs/1703.08246

[28] ITU-R, "P.1411-6: Propagation data and prediction methods for the planning of short-range outdoor radiocommunication systems and radio local area networks in the frequency range 300 MHz to 100 GHz," Feb. 2012.

[29] H. Tabassum, Z. Dawy, E. Hossain, and M. S. Alouini, "Interference statistics and capacity analysis for uplink transmission in two-tier small cell networks: A geometric probability approach," *IEEE Transactions on Wireless Communications*, vol. 13, no. 7, pp. 3837–3852, July 2014.

[30] M. Taranetz and M. Rupp, "A circular interference model for heterogeneous cellular networks," *IEEE Transactions on Wireless Communications*, vol. 15, no. 2, pp. 1432–1444, Feb. 2016.

[31] H. Tabassum, F. Yilmaz, Z. Dawy, and M. S. Alouini, "A statistical model of uplink inter-cell interference with slow and fast power control mechanisms," *IEEE Transactions on Communications*, vol. 61, no. 9, pp. 3953–3966, Sep. 2013.

[32] H. ElSawy and E. Hossain, "On stochastic geometry modeling of cellular uplink transmission with truncated channel inversion power control," *IEEE Transactions on Wireless Communications*, vol. 13, no. 8, pp. 4454–4469, Aug. 2014.

Ming Ding (M'12-SM'17) received the B.S. and M.S. degrees (with first class Hons.) in electronics engineering from Shanghai Jiao Tong University (SJTU), Shanghai, China, and the Doctor of Philosophy (Ph.D.) degree in signal and information processing from SJTU, in 2004, 2007, and 2011, respectively. From April 2007 to September 2014, he worked at Sharp Laboratories of China in Shanghai, China as a Researcher/Senior Researcher/Principal Researcher. He also served as the Algorithm Design Director and Programming Director for a system-level simulator of future telecommunication networks in Sharp Laboratories of China for more than 7 years. Currently, he is a senior research scientist at Data61, CSIRO, in Sydney, NSW, Australia. He has authored more than 50 papers in IEEE journals and conferences, all in recognized venues, and about 20 3GPP standardization contributions, as well as a Springer book "Multi-point Cooperative Communication Systems: Theory and Applications". Also, as the first inventor, he holds 15 CN, 7 JP, 3 US, 2 KR patents and co-authored another 100+ patent applications on 4G/5G technologies. He is or has been Guest Editor/Co-Chair/Co-Tutor/TPC member of several IEEE top-tier journals/conferences, e.g., the IEEE Journal on Selected Areas in Communications, the IEEE Communications Magazine, and the IEEE Globecom Workshops, etc. For his inventions and publications, he was the recipient of the President's Award of Sharp Laboratories of China in 2012, and served as one of the key members in the 4G/5G standardization team when it was awarded in 2014 as Sharp Company Best Team: LTE 2014 Standardization Patent Portfolio.

David López-Pérez (M'12-SM'17) is currently a member of Technical Staff at Nokia Bell Laboratories. Prior to this, David received the B.Sc. and M.Sc. degrees in telecommunication from Miguel Hernandez University, Spain, in 2003 and 2006, respectively, and the Ph.D. degree in wireless networking from the University of Bedfordshire, U.K., in 2011. David was also a RF Engineer with Vodafone, Spain, from 2005 to 2006, and a Research Associate with King's College London, U.K., from 2010 to 2011. David has authored the book "Heterogeneous Cellular Networks: Theory, Simulation and Deployment" (Cambridge University Press, 2012), as well as over 100 book chapters, journal, and conference papers, all in recognized venues. He also holds over 36 patents applications. David received the Ph.D. Marie-Curie Fellowship in 2007 and the IEEE ComSoc Best Young Professional Industry Award in 2016. He was also a finalist for the Scientist of the Year prize in The Irish Laboratory Awards in 2013 and 2015. He is an editor of IEEE TRANSACTION on WIRELESS COMMUNICATIONS since 2016, and he was awarded as Exemplary Reviewer of the IEEE COMMUNICATIONS LETTERS in 2011. He is or has also been a Guest Editor of a number of journals, e.g., the IEEE JOURNAL ON SELECTED AREAS IN COMMUNICATIONS, the IEEE Communication Magazine and the IEEE Wireless Communication Magazine.

Guoqiang Mao (S'98-M'02-SM'08) joined the University of Technology Sydney in February 2014 as Professor of Wireless Networking and Director of Center for Real-time Information Networks. Before that, he was with the School of Electrical and Information Engineering, the University of Sydney. He has published about 200 papers in international conferences and journals, which have been cited more than 5000 times. He is an editor of the IEEE Transactions on Wireless Communications (since 2014), IEEE Transactions on Vehicular Technology (since 2010) and received "Top Editor" award for outstanding contributions to the IEEE Transactions on Vehicular Technology in 2011, 2014 and 2015. He is a co-chair of IEEE Intelligent Transport Systems Society Technical Committee on Communication Networks. He has served as a chair, co-chair and TPC member in a large number of international conferences. He is a fellow of IET. His research interest includes intelligent transport systems, applied graph theory and its applications in telecommunications, Internet of Things, wireless sensor networks, wireless localization techniques and network performance analysis.

This article has been accepted for publication in a future issue of this journal, but has not been fully edited. Content may change prior to final publication. Citation information: DOI 10.1109/TCOMM.2017.2751552, IEEE Transactions on Communications

Zihuai Lin (S'98-M'06-SM'10) received the Ph.D. degree in Electrical Engineering from Chalmers University of Technology, Sweden, in 2006. Prior to this he has held positions at Ericsson Research, Stockholm, Sweden. Following Ph.D. graduation, he worked as a Research Associate Professor at Aalborg University, Denmark and currently at the School of Electrical and Information Engineering, the University of Sydney, Australia. His research interests include source/channel/network coding, coded modulation, MIMO, OFDMA, SC-FDMA, radio resource management, cooperative communications, small-cell networks, 5G cellular systems, IoT, etc.

Sajal K. Das (M'96-SM'08-F'15) is a professor of Computer Science Department and the Daniel St. Clair Endowed Chair at the Missouri University of Science and Technology, USA. His current research interests include wireless and sensor networks, cyber-physical systems, smart grid and smart healthcare, distributed and cloud computing, big data and IoT, security, biological and social networks, applied graph theory and game theory. He serves as the founding Editor-in-Chief of Elsevier's Pervasive and Mobile Computing Journal, and as Associate Editor of IEEE Transactions on Mobile Computing and ACM Transactions on Sensor Networks.